

Supporting Information

Green DES-mediated preparation of rose-shaped S-scheme heterojunction photocatalyst (β - $\text{Bi}_2\text{O}_3/\text{Bi}_2\text{O}_{2.33}$)/ TiO_2 to boost antibiotics degradation

Xiaoyun Zhu,[#] Yongjiao Hu,[#] Lijia Wang, Xuhua Wang, Yingqiang Zhao, Qikun Zhang, Pin Hao,* Qian Wang*

College of Chemistry, Chemical Engineering and Materials Science, Institute of Materials and Clean Energy, Collaborative Innovation Center of Functionalized Probes for Chemical Imaging in Universities of Shandong, Key Laboratory of Molecular and Nano Probes, Ministry of Education, Shandong Provincial Key Laboratory of Clean Production of Fine Chemicals, Shandong Normal University, Jinan 250014, P. R. China.

*Corresponding author:

haopin@sdnu.edu.cn, wangqian@sdnu.edu.cn

[#]These authors contributed equally.

1. Experimental Section
2. Figures
3. References

1. Experimental Section

1.1 Materials

Lactic acid, choline chloride (ChCl) and ethanol were purchased from Sinopharm Group Chemical Reagent Co., Ltd., Beijing, China. Tetrabutyl titanate (TBOT), tetracycline (TC), ofloxacin (OFLX), amoxicillin (AMX) and ciprofloxacin (CPFX) were provided by Macklin Biochemical Co., Ltd., Shanghai, China. All the reagents are utilized without any purification.

1.2 Synthesis of DES

Deep Eutectic Solvents (DESs) are eutectic compounds usually obtained by mixing hydrogen bond acceptors (HBAs) and hydrogen bond donors (HBDs) *via* hydrogen-bond association.^[7,S1] They mainly have the following advantages over conventional solvents in nanomaterial synthesis: (I) The structures and properties of DESs can be easily adjusted by selecting both the nature and the ratio of the hydrogen-bonding constituents. (II) The extensive hydrogen-bond networks in DESs enable the template effect for regulating crystal growth of materials. (III) DES has high solubility and can dissolve a variety of organic and inorganic compounds to provide a stable dispersion system that ensures complex syntheses go smoothly.^[S2-S4] In this work, DES was synthesized by mixing three components ChCl, urea and lactic acid with 2:1:1 molar ratio to form a clear and transparent liquid at 80 °C under continuous stirring for 2 h. Fourier transform infrared (FT-IR) spectra of ChCl, urea, lactic acid and the designed ChCl/urea/lactic acid DES are shown in Fig. S1. The –NH₂ vibration of urea and –OH

vibration of lactic acid in the DES showed obvious red shifts from 3433 (3340) and 3416 to 3316 cm^{-1} , while the $-\text{OH}$ vibration of ChCl in the DES displayed an evident blue shift from 3226 to 3316 cm^{-1} , which illustrated that H-bonding chiefly took place between H in the $-\text{NH}_2$ of urea and the Cl^- of ChCl (or O in the $-\text{OH}$ of ChCl), between H in the $-\text{OH}$ of lactic acid and the Cl^- of ChCl , and between O in the $-\text{OH}$ of lactic acid and H in the $-\text{OH}$ of ChCl .^[10]

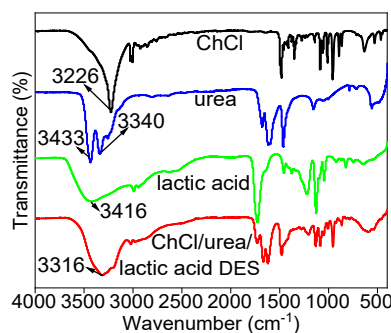


Fig. S1. FT-IR spectra of ChCl , urea, lactic acid and the $\text{ChCl}/\text{urea}/\text{lactic acid}$ DES.

1.3 Synthesis of ($\beta\text{-Bi}_2\text{O}_3/\text{Bi}_2\text{O}_{2.33}$)/ TiO_2 (BBOTO)

Firstly, 1.5 mL distilled water was added into 13.5 mL DES with vigorous string to obtain a mixed solution which play the role of reaction solvent and structure oriented template. Then, 0.02 mmol $\text{Bi}(\text{NO}_3)_3 \cdot 5\text{H}_2\text{O}$ and 0.25 mmol tetrabutyl titanate (TBOT) as raw materials were added into the mixed solution in turn. Then the obtained mixture was transferred to a 25 mL Teflon-lined stainless-steel autoclave at 180 $^\circ\text{C}$ for 18 h. After being naturally cooled to room temperature, the mixture was subsequently washed repeatedly with distilled water and absolute ethanol, collected to obtain a white precipitate, and dried in an oven at 60 $^\circ\text{C}$ for 12 h. Finally, the collected powder was calcined at 400 $^\circ\text{C}$ for 4 h in air atmosphere to obtain the target samples (BBOTO). The sample with lower content of oxygen vacancies was prepared by changing the

calcination temperature (at 420 °C), which was named as BBOTO-1. Moreover, the pure β - $\text{Bi}_2\text{O}_3/\text{Bi}_2\text{O}_{2.33}$ (abbreviated to BBO), and pure TiO_2 (abbreviated to TO) were also synthesized, and their synthesized steps are the same with that of BBOTO apart from only adding Bi source $\text{Bi}(\text{NO}_3)_3 \cdot 5\text{H}_2\text{O}$ or Ti source TBOT.

1.4 Characterizations of DES and catalyst

FT-IR spectra were characterized with a Varian 3100 FT-IR spectrometer. The crystal structure of the sample was determined by an X-ray diffractometer (XRD, Bruker D8, Germany) using $\text{Cu K}\alpha$ radiation. The morphology and microstructure of the sample were examined by scanning electron microscopy (SEM, Hitachi S4800), transmission electron microscopy (TEM) and High-Resolution TEM (HRTEM, JEM 2010 EX). Nitrogen adsorption/desorption curves were collected by a Micromeritics ASAP2020. X-ray photoelectron spectroscopy (XPS) spectra were collected on a Thermo Scientific Escalab250Xi spectrometer equipped with an $\text{Al K}\alpha$ Source (1486.6eV). Diffuse reflectance spectroscopy (DRS) spectrum of samples and the absorption intensity of antibiotic were measured by an UV-Vis spectrometer (METASH UV-8000). Electron paramagnetic resonance (EPR) spectra were recorded on a Bruker A300 spectrophotometer. Photoelectric chemical measurements were measured in a standard three-electrode system on the electrochemical workstation (CHI660E, Chenhua, China).

1.5 Photocatalytic activity test

TC was selected as the main model pollutant to investigate the photocatalytic activities of the synthesized catalysts. Typically, 5 mg catalysts were added into a quartz

tube containing 25 mL antibiotic solution ($C_0=10$ mg/L) at room temperature, the obtained mixture was stirred in darkness for 45 min, and then the mixture was placed under a 500 W xenon lamp for photocatalytic reaction. After the reaction, the supernatant was obtained by centrifugation. The absorption intensity of the supernatant was measured by UV-VIS spectrophotometer at 276 nm, and the degradation rate of TC was calculated. The catalytic degradation conditions of OFLX, AMX and CPFX were the same as that of TC, while its absorption intensities were tested at 288, 283 and 272 nm, respectively.

The photocatalytic H_2 evolution experiment was carried out in a 30 mL quartz vessel sealed with a silicone rubber septum at an ambient temperature under atmospheric pressure. First, 5 mg of the as-prepared photocatalysts, was suspended in 10 mL double distilled water containing 30 vol% methanol as the sacrificial electron donor. Then the sample solution was thoroughly deaerated by evacuation and purged with nitrogen for 20 min. Next a 500 W Xe lamp was irradiated for 6 h at room temperature under constant stirring. Finally, the evolved gases were analyzed by injecting 1 mL of headspace gas into the gas chromatograph (FULI 9750, TCD, Nitrogen as the carrier gas, and 5 Å molecular sieve column).

1.6 Photoelectrochemical performance measurement

Using catalyst electrode, Ag/AgCl electrode, and Pt wire electrode as the working electrode, reference electrode and counter electrode, respectively, 0.5 M Na_2SO_4 solution as the electrolyte, photocurrent responses test was carried out under 350 W Xenon lamp illumination with a bias voltage of 0.6 V. Selecting catalyst electrode,

mercury/mercuric oxide electrode and Pt wire electrode as the working electrode, reference electrode and counter electrode, respectively, 1 M NaOH solution as the electrolyte, electrochemical impedance spectroscopy (EIS) was carried out at open circuit voltage over a frequency range of 0.01-100000 Hz with a bias voltage of 0.5 V.

2. Figures

2.1 UV-DRS spectra and the corresponding band gap energies

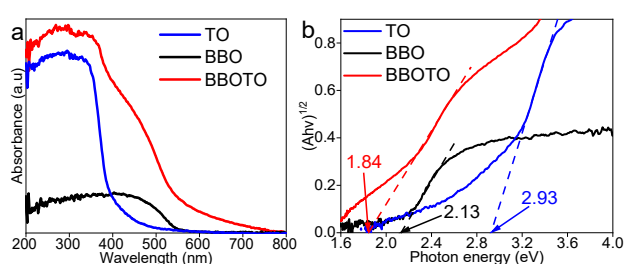


Fig. S2. (a) UV-DRS spectra and (b) the corresponding band gap energies of pristine TO, pristine BBO and BBOTO.

2.2 XRD pattern and high resolution XPS spectra O 1s of BBOTO-1

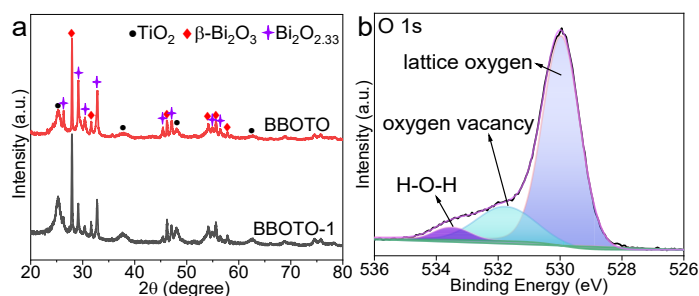


Fig. S3. (a) XRD patterns of BBOTO and BBOTO-1. (b) High resolution XPS spectrum O 1s of

BBOTO-1.

The XRD pattern of BBOTO-1 in Fig. S3a showed the same positions of characterizational peaks with that of BBOTO. The contents of oxygen vacancies of BBOTO and BBOTO-1 were calculated as 22.85 % and 18.28 % based on the high-

resolution XPS spectra of O1s of the two catalysts in Fig. 2d and Fig. S3b by the

formula of $O_{\text{oxygen vacancies}} / (O_{\text{lattice oxygen}} + O_{\text{oxygen vacancies}} + O_{\text{surface absorbed hydroxyl}})$.^[S5,S6]

2.2 TC photodegradation curves with different oxygen vacancy contents

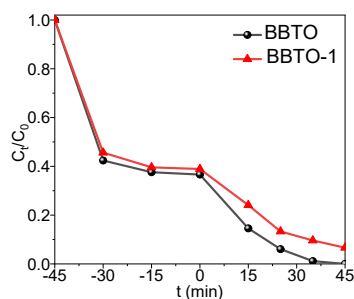


Fig. S4. TC photodegradation curves BBOTO and BBOTO-1.

2.2 Comparison of degradation rate with reported values

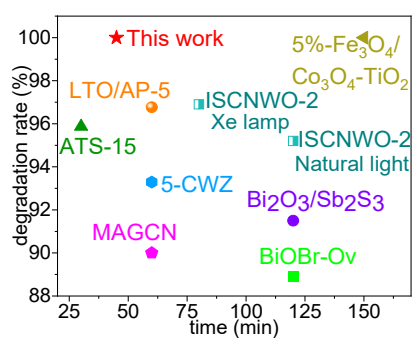


Fig. S5. Comparison of degradation rate with reported values.^[S7-S14]

2.3 Stability test

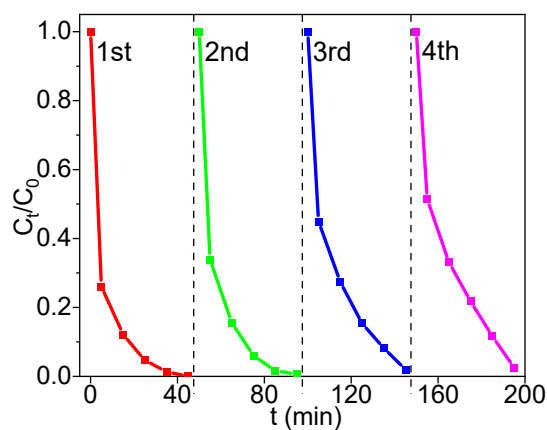


Fig. S6. Stability test of BBOTO.

2.4 TPR and EIS spectra

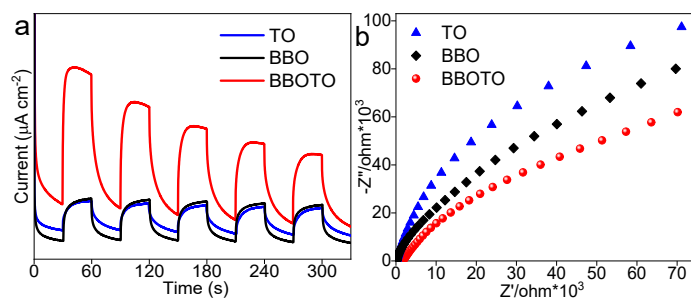


Fig. S7. (a) TPR, (b) EIS Nyquist plots of individual TO, individual BBO and BBOTO.

3. References

- [S1] N.V.P. Veríssimo, C.U. Mussagy, H.B.S. Bento, J.F.B. Pereira, V.d.C. Santos-Ebinuma, *Biotechnol. Adv.*, 2024, **71**, 108316.
- [S2] Y. Ma, Y. Yang, T. Li, S. Hussain, M.Y. Zhu, *Green Chem.*, 2024, **26**, 3627.
- [S3] B.B. Hansen, S. Spittle, B. Chen, D. Poe, Y. Zhang, J.M. Klein, A. Horton, L. Adhikari, T. Zelovich, B.W. Doherty, B. Gurkan, E.J. Maginn, A. Ragauskas, M. Dadmun, T.A. Zawodzinski, G.A. Baker, M.E. Tuckerman, R.F. Savinell, J.R. Sangoro, *Chem Rev.*, 2021, **121**, 1232.
- [S4] R.R. Deng, M.G. Gao, B. Zhang, Q.B. Zhang, *Adv. Energy Mater.*, 2024, **14**, 2303707.
- [S5] J. Cao, S. Rohani, W.Z. Liu, H.H. Liu, Z.Q. Lu, H.L. Wu, L.J. Jiang, M. Kong, Q. C. Liu, X.J. Yao, *J. Colloid Interf. Sci.*, 2022, **610**, 463.
- [S6] L.M. Luo, J.B. Zhong, J. Z.Li, *Mater. Res. Bull.*, 2022, **150**, 111763.
- [S7] W.H. Zhang, Z.Y. Bian, Y.Y. Peng, H.Y. Tang, H. Wang, *Chem. Eng. J.*, 2023, **451**, 138731.
- [S8] C.Y. Teng, Y.Y. Chen, Z.J. Tang, W.Y. Yuan, L. Zhang, Y.F. Guo, F. Li, Q. Huang, *Chem. Eng. J.*, 2024, **488**, 150983.
- [S9] H.B. Sun, P.F. Qin, J.Y. Guo, Y. Jiang, Y.S. Liang, X.M. Gong, X. Ma, Q. Wu, J.C. Zhang, L. Luo, Z.B. Wu, *Chem. Eng. J.*, 2023, **470**, 144217.
- [S10] C. Maggu, S. Singla, S. Basu, *J. Environ. Manage.*, 2024, **349**, 119424.
- [S11] H.M. Lu, X.Y. Li, Y. Jiang, X.L. Hu, S.F. Zhou, H.B. Sun, D.S. Zou, Y.S. Liang, X.M. Gong, Z.B. Wu, *Chem. Eng. J.*, 2023, **476**, 146718.

[S12] S. Kumaravel, D.S. Lee, T. Niyitanga, S. Kaliyamoorthy, I. Hasan, K. Balu, *J. Alloy. Compd.*, 2024, **994**, 174666.

[S13] X.J. Chen, J.M. Chen, N. Li, J.S. Li, J.H. He, S. Xu, Y.P. Zhu, L. Yao, Y.Q. Lai, R.L. Zhu, *Environ. Pollut*, 2023, **323**, 121322.

[S14] M.M. Abutalib, H.M. Alghamdi, A. Rajeh, O. Nur, A.M. Hezma, M.A. Mannaa, *J. Mater. Res. Technol.*, 2022, **20**, 1043.